Self-Assembly of Block Copolymers for Photonic-Bandgap Materials

Jongseung Yoon, Wonmok Lee, and Edwin L. Thomas

Abstract

Self-assembled block copolymer systems with an appropriate molecular weight to produce a length scale that will interact with visible light are an alternative platform material for the fabrication of large-area, well-ordered photonic-bandgap structures at visible and near-IR frequencies. Over the past years, one-, two-, and three-dimensional photonic crystals have been demonstrated with various microdomain structures created through microphase separation of block copolymers. The size and shape of periodic microstructures of block copolymers can be readily tuned by molecular weight, relative composition of the copolymer, and blending with homopolymers or plasticizers. The versatility of photonic crystals based on block copolymers is further increased by incorporating inorganic nanoparticles or liquid-crystalline guest molecules (or using a liquid-crystalline block), or by selective etching of one of the microdomains and backfilling with high-refractive-index materials. This article presents an overview of photonic-bandgap materials enabled by self-assembled block copolymers and discusses the morphology and photonic properties of block-copolymer-based photonic crystals containing nanocomposite additives. We also provide a view of the direction of future research, especially toward novel photonic devices.

Keywords: *block copolymers, nanocomposites, photonic crystals.*

Introduction

Block copolymers (BCPs), molecules comprising chemically distinct polymer chains connected to each other, self-assemble to create a variety of periodic structures.[1] The self-assembly of BCPs is driven by a competition between the positive enthalpy of mixing of the respective block chains and the tendency for the polymers to desire a random coil configuration.[2] When χN is larger than a certain value (e.g., 10.5 for symmetric diblocks), where χ is the Flory–Huggins interaction parameter between blocks and N is the total degree of polymerization (equal to the total numbers of A monomers and B monomers) of the BCP, microphase separation into well-defined domain structures occurs on the length scale of the respective blocks. For example, in the case of simple linear A–B diblock copolymers, χN and the volume fraction f determine the four equilibrium morphologies: lamellae, double gyroid networks, hexagonally packed cylinders, and bcc spheres. The diversity of BCP microstructures in terms of microdomain size and shape is greatly increased by changing the number of components, the architecture, or the persistence length (a measure of the local straightness) of the constituting chains, or by blending with additives (homopolymers, plasticizers, etc.). For example, A–B–C terpolymers, in which three chemically different blocks are either connected in a series via two junctions or connected to a single junction to form miktoarm ("mixed arm") star polymers, exhibit a range of more complex morphologies compared with simple diblock copolymers (see the article by Bates in the July 2005 issue of *MRS Bulletin*). The wide range of microstructures accessible from the self-assembly of BCPs has made them excellent candidate materials for numerous nanotechnological applications, including photonic-bandgap materials.[1,3]

Recently, photonic crystals have become of great interest for researchers because of their unique electromagnetic properties, particularly their ability to trap and guide light, thus promising many applications in the fields of optical communication, sensing, and optical limiting.[4-6] Photonic crystals are defined as ordered structures with a periodic variation of the dielectric constant.[7] The spatial periodicity and dimensionality of the crystal determine the photonic bandgap, a range of frequencies in which the propagation of electromagnetic waves is prohibited in certain directions. Experimentally, a variety of methods have been proposed to construct photonic crystals to work at near-IR and optical frequencies. Lithographic methods based on semiconductor fabrication techniques using masks have been utilized to make 2D photonic crystals and even some 3D photonic crystals, although fabrication of 3D photonic crystals by this approach requires many processing steps.[8,9] Holography or interference lithography holds much promise, especially for making 3D photonic structures with much less effort than conventional lithographic tools.[10,11]

Besides these *top-down* lithographic approaches, *bottom-up* self-assembly methods have also been actively pursued for making photonic-bandgap structures. Synthetic opals made of spherical silica or polymeric colloidal particles have been extensively studied.[12,13] The closed-packed structures yield the fcc structure or, after infiltration by a second material and removal of the original spheres, the inverse fcc structure.[14] More recently, BCPs have emerged as another platform material for fabricating photonic crystals, because of their inherent flexibility in accessing a variety of 1D, 2D, and 3D periodic structures; their ability to incorporate a wide choice of materials, including the possibility of high-dielectric and optically active nanoparticle additives; and their relatively straightforward, cost-effective processing.

This article will review recent progress in the development of photonic-bandgap materials enabled with the self-assembly of BCPs, discussing the morphology and photonic properties of these BCP-based photonic materials including BCP–nano-

particle composites. In addition, a perspective view to the direction of future research, especially toward novel photonic devices based on the block polymer materials platform, will be presented.

1D, 2D, and 3D Block Copolymer Photonic Crystals

Photonic crystals will be an important part of future optical systems. For example, a discrete region of different index or geometry that serves to break the symmetry inside the photonic crystal can serve as an optical cavity, while a line defect can act as a waveguide and a surface defect can act like a mirror. As these features are all on the size scale of the periodicity, this affords both integration and miniaturization of optical devices. Even the most basic photonic crystal, a 1D multilayer stack in which the dielectric constant varies along only one direction, can act as a notch filter (a filter that can pass a narrow wavelength range of incident light) by incorporating a single defect layer in the stack. Multilayer devices are normally fabricated by various layer-by-layer approaches such as electron-beam, sputtering, or vacuum deposition methods using two sources and two shutters to control the thicknesses of the alternating layers in the stack. Another way to produce multilayer structures is by BCP lamellar self-assembly.

Since BCPs of typical molecular weight (~50 kg/mol) form microdomains on a typical length scale (~20 nm), the domain spacing is insufficient for optical applications. What is needed in order to produce a bandgap at visible or near-IR wavelengths is to increase the average domain size, on the order of $\lambda/4n_i$, where n_i is the index of refraction of the respective block and λ is the wavelength of light. For 600 nm visible (red) light, and for a typical polymer index of 1.5, this calls for an individual block layer thickness of approximately 100 nm, requiring a block molecular weight of ~500 kg/mol and a total polymer molecular weight of around 1000 kg/mol. Such large domain spacings can also be accessed by employing somewhat lower-molecular-weight copolymers (e.g., ~200 kg/mol per block) and swelling the respective domains by blending with low-molecular-weight homopolymers or nonvolatile plasticizers, or by employing rigid, rodlike polymers with a large persistence length.

The first example of a visible BCP photonic crystal was achieved by using symmetric poly(styrene-*b*-isoprene) (PS–PI) diblock copolymers with approximate molecular weights of 200 kg/mol per block and forming a 60/20/20 ternary blend with the respective homopolymer of each block.[15–17] Indeed, the systematic blending of low-molecular-weight homopolymers into the host BCP provides a way to tune the photonic bandgap (the so-called "stop band") across the entire visible wavelength range by simply controlling the amount of blended homopolymers (Figure 1a).[17]

A convenient way to understand the optical properties of a photonic crystal is

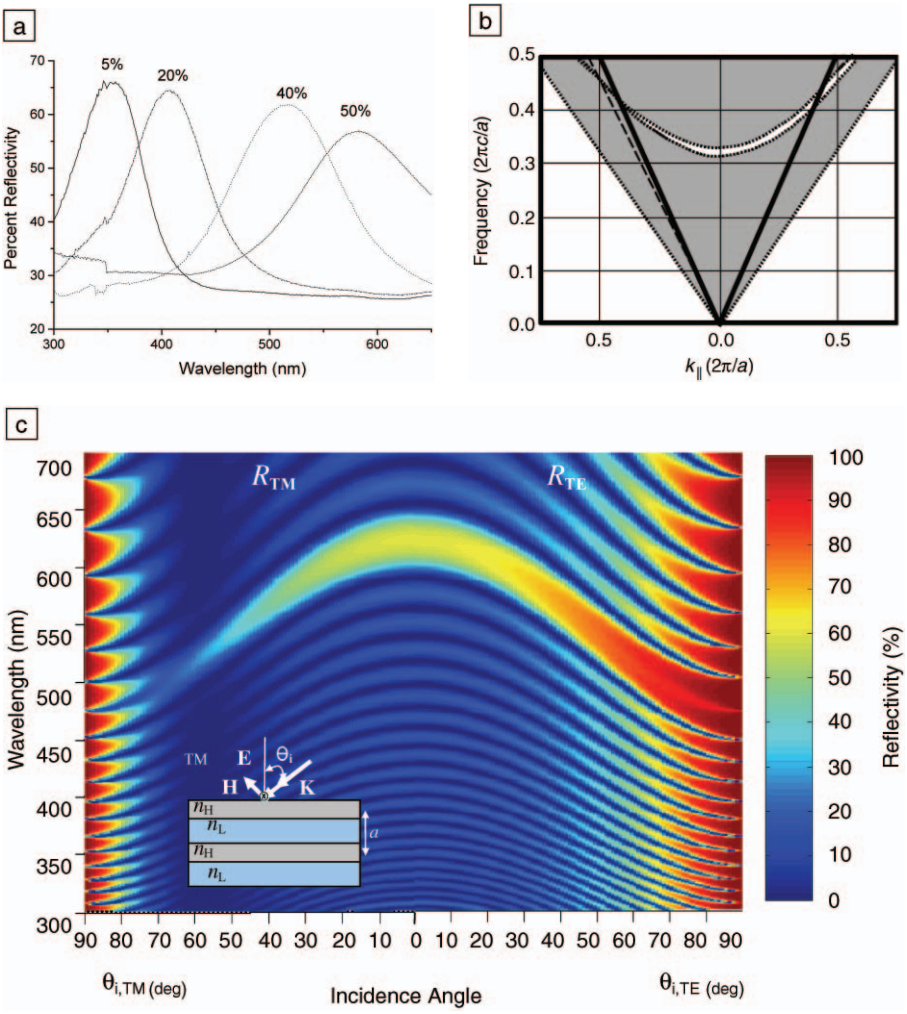

*Figure 1. (a) Reflectivity of ternary block copolymer (PS–PI with 194 kg/mol of PS block and 197kg/mol of PI block)/homopolymer (13kg/mol of PS and 13kg/mol of PI) blends containing 5%, 20%, 40%, and 50% added homopolymer, respectively. The progression of the stop band to longer wavelengths and broader peaks with increasing homopolymer content is evident. (Reprinted with permission from Reference 17.) (b) A band diagram (dimensionless frequency versus dimensionless wave vector) using the refractive indices of polystyrene (PS) and polyisoprene (PI) and the layer thicknesses of a PS-b-PI/PS/PI blend (c is the speed of light in a vacuum, a is the lamellar domain periodicity). The transverse-electric (TE) polarization modes are on the right side, and the left side is for the transverse-magnetic (TM) polarized light. The shaded regions represent allowed propagating modes. The dotted curves are the band edges. The partial bandgap is the thin, crescent-shaped region between the second and third bands. The region between the solid black lines (the "light lines") defines the region of the diagram accessible to light incident from outside the material. The dashed curve on the left side of the graph is the Brewster line, the angle where TM polarized light passes through the structure without reflection. (Reprinted with permission from Reference 16.) (c) Reflectivity plot constructed by the transfer matrix method for a 20-period stack of alternating PS and PI layers, where R_{TM} and R_{TE} represent the reflectivity for TM and TE polarization, respectively. Each layer is assumed to be 100 nm thick. The color represents the strength of the reflectivity at a particular frequency and angle of incidence. The inset shows a schematic of TM polarized light incident on the multilayer stack with an angle θ_i (**E** = electric field vector, **H** = magnetic field vector, **k** = wave vector, n_H = refractive index of high-index layer, n_L = refractive index of low- index layer, a = domain periodicity).*

to examine the dispersion relationship between the frequency ω of incident light and the direction of the wave vector **k**. If we consider an infinite periodic medium, the ω(**k**) relationship can be derived from solutions to Maxwell's equations and is displayed as a band diagram. The dispersion relationship of a 1D photonic crystal has been analytically derived by Yeh et al.[18] Figure 1b is an illustration of the band diagram for a multilayer system with layer thicknesses and refractive indices typical of polystyrene and polyisoprene, and provides information on sample reflectivity as a function of incidence angle and polarization of the incident electromagnetic waves.[16] The shaded areas on the diagram represent propagating modes, while the white areas represent the non-propagating evanescent modes. Light in the range of wavelengths represented by the white areas incident for the particular **k** vector is reflected by constructive interference from the set of periodically spaced interfaces between the two types of domain. The plot also shows how the center wavelength of the bandgap is shifted to a shorter wavelength as the incidence angle moves from normal toward grazing. Thus, a film appearing green when viewed at normal incidence appears blue when viewed at an angle far off the normal. A second way to view the same sort of reflectance data for a *finite* photonic crystal is to plot the magnitude of the reflectivity—which depends on the dielectric contrast ($\varepsilon_2/\varepsilon_1$) and, importantly, on the number of periods in the photonic crystal—as a function of wavelength and incident angle (see Figure 1c). This type of calculation can be done using the transfer matrix method,[19] which also allows one to include finite material absorption in the calculation as well as optical anisotropy.

Two-dimensionally periodic BCP photonic crystals have been also demonstrated using self-assembly. In this case, a cylinder-forming PS–PI diblock copolymer was roll-cast to realize a long-range-ordered 2D periodic photonic crystal structure.[20] The bandgap exists in the plane of the domain periodicity; thus, light propagating perpendicular to the cylinder axis is reflected. The small dielectric contrast (~1.1) produced only a partial photonic bandgap. In order to achieve a complete bandgap for both transverse-electric (TE) and transverse-magnetic (TM) polarizations in the hexagonal cylinder structure, a minimum dielectric contrast of 7.2:1 is necessary. This illustrates the challenge to somehow access a much higher dielectric contrast than is inherent to polymeric systems.

A three-dimensionally periodic photonic crystal with a complete photonic bandgap in the optical or near-IR frequencies has been one of the main challenges for researchers since the inception of the field in 1987.[21,22] Yablonovitch first proposed that a fcc arrangement of dielectric cubes would provide the sought-after complete bandgap.[23] Researchers attempted to create such a fcc photonic crystal structure using close-packed spheres, but the bandgap occurs at a relatively low volume fraction of dielectric, so infiltration of a high-dielectric material about a template of fcc packed spheres was performed, followed by etching to create an air lattice of spheres in a high dielectric.[14] Unfortunately, the fcc structure does not have a complete bandgap between low-order bands, and the complete gap opens up between the eighth and ninth bands only at a relatively large dielectric contrast of nearly 9:1.[24]

Since then, researchers have sought alternative structures that would provide a robust gap at a lower dielectric contrast that could also be readily fabricated. Interestingly, the current champion photonic-crystal structure is that of an interconnected network with a diamond crystal structure first discovered by the Iowa State University group in 1991.[25] The 34 vol% diamond dielectric network displays a complete bandgap between the second and third bands at the record low dielectric contrast of 3.6:1 (note that attaining an index contrast of $\sqrt{3.6}$:1 = 1.9:1 in a polymer:air diamond network structure is not out of the question).

Block polymers can provide many possible intricate 3D structures through microphase separation. The first 3D BCP photonic crystal having a partial photonic bandgap was based on the bicontinuous double gyroid cubic morphology (Figure 2a).[26] Here a PS–PI BCP with total molecular weight of 750 kg/mol provided domain sizes sufficient to interact with visible light (Figure 2b).[26] The double gyroid morphology was further treated with UV and ozone to degrade the polyisoprene phase, leaving the polystyrene double gyroid network with increased refractive-index contrast (polystyrene versus air, 1.6:1) (Figure 2c).[26]

However, it turns out that the double gyroid network structure does not possess

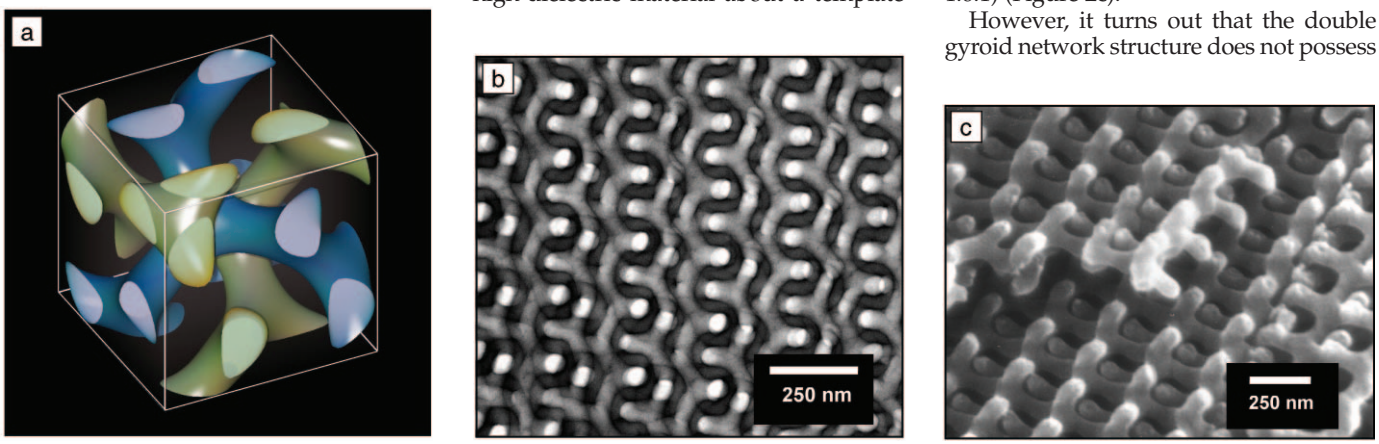

Figure 2. (a) Schematic illustration of the unit cell of the double gyroid morphology. The double gyroid structure comprises two interpenetrating three-dimensionally continuous networks of the minority component (shown in blue and yellow to help in visualization). (b) Transmission electron micrograph of an 80-nm-thick cryo-microtomed thin section of the 750 kg/mol PS–PI block copolymer. The image is of the [123] projection of the microstructure, yielding a lattice parameter of the cubic cell of 250 nm. The isoprene matrix has been stained with osmium tetroxide, leaving the styrene networks light in this bright-field micrograph. (Reprinted with permission from Reference 26.) (c) Scanning electron microscopy secondary electron image of the double gyroid styrene networks remaining after UV/ozone etching, showing that the networks remain intact and self-supporting after processing. The dimensions of the network structure are not perceptibly changed by the processing. (Reprinted with permission from Reference 26.)

a complete gap, no matter how high the dielectric contrast. This makes clear the need to perform simulations of potential structures to explore for robust bandgaps prior to undertaking extensive experiments. We have used numerical calculations employing the plane wave method[24] to examine a host of network structures having various cubic symmetries.[27] What is done is to systematically explore the range of volume fractions and dielectric contrasts for a given structure to see if it displays a complete gap and then to construct a "gap map"—that is, a plot of the width of the complete gap (the difference in frequency of the lowest frequency of the upper band and the highest frequency of the lower band versus dielectric contrast at a fixed volume fraction). Of particular concern is finding the structure and the volume fraction of the structure at which a complete gap first opens at the lowest possible dielectric contrast. This volume fraction will give the widest gap for a given dielectric contrast. It is noteworthy that neither the double gyroid nor the double diamond structures exhibit complete bandgaps, while both of the corresponding single network structures do, with the single diamond network as the current *champion* complete-gap structure. The single gyroid morphology is also a favorable photonic crystal structure—a complete photonic bandgap opens at a index contrast of 2.3:1 (Figure 3).[27]

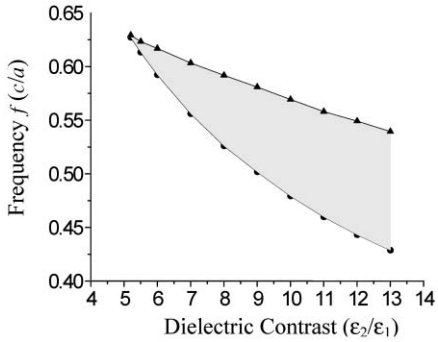

Figure 3. The single gyroid dielectric network "gap map" generated for the 17% high-dielectric network volume fraction, showing the gap opening at a dielectric contrast of 5.2, and a maximum gap width of approximately 25% at a contrast of 13:1. The 17% network is precisely half of a 34% volume fraction double gyroid morphology observed in block copolymers. The solid triangles (▲) and solid circles (●) represent the frequencies at the high- and low-frequency edge of the photonic bandgap, respectively. ε_2 is the dielectric constant of the high-index material, ε_1 is the dielectric constant of the low-index material, c is the speed of light in a vacuum, a is the lattice parameter of single gyroid structure.

Nanocomposite Block Copolymer Photonic Materials

Given the inherently low dielectric contrast in BCP-based photonic crystals (typically on the order of 1.1:1 for polymer:polymer structures and 1.5:1 for polymer:air structures) it is essential to enhance the dielectric contrast in order to produce a more robust (or even complete) photonic bandgap. One method that has been successfully demonstrated is to sequester high-refractive-index inorganic nanocrystals into the microdomains of a BCP to form an inorganic/organic microstructured nanocomposite photonic structure. For example, CdSe particles with trioctyl phosphine oxide (TOPO) surface ligands (CdSe refractive index, ~2.7) were successfully sequestered into the poly(vinyl pyridine) domains in a poly(styrene-*b*-isoprene-*b*-vinyl pyridine) block terpolymer.[15] In order to target the high-index nanoparticles to the higher-index block domains, one needs to tailor the nanocrystal surface to have compatibilizing groups (typically oligomeric homopolymers) similar to the host block domains. Thus, amine- or thiol-terminated polystyrene was used to compatibilize CdSe nanocrystals into PS–PI BCPs by ligand-exchange reactions. Since the electronic bandgap of semiconductor nanocrystals is inversely proportional to the size of the nanocrystals, the absorption band of nanocrystals is shifted to a shorter wavelength than in bulk materials, making the nanocrystals effectively transparent in the optical regime.

Metallic nanoparticles are also of interest for their extremely high dielectric constants. The optical response of BCP/metallodielectric nanocrystal photonic structures can also be dramatically influenced by the spatial distribution of metallodielectric nanocrystals because of the dipolar coupling between closely spaced metal particles. For example, a metallodielectric photonic structure based on poly(styrene-*b*-ethylene/propylene) diblock copolymer and gold nanocrystals was coassembled using gold nanocrystals with a size well below the scattering limit.[28–30] The gold particles were surface-grafted with different chemical groups, such as thiol-terminated oligomeric polystyrene (AuSPS) or thiol-terminated alkanes (e.g. $AuSC_{18}H_{37}$), to target a given type of microdomain in the BCP template. Two distinct spatial distributions of gold nanocrystals were observed: (1) interfacial segregation between the two block domains, and (2) preferential uniform distribution within one type of domain. These morphologies were dependent on the surface chemistry and size of the ligands attached to the particles, as shown in Figure 4.[30] The confinement of the nanocrystals to the narrow interface between domains results in a high local particle concentration and therefore a small average distance between particles, leading to different optical properties of the respective nanocomposite structures.[30]

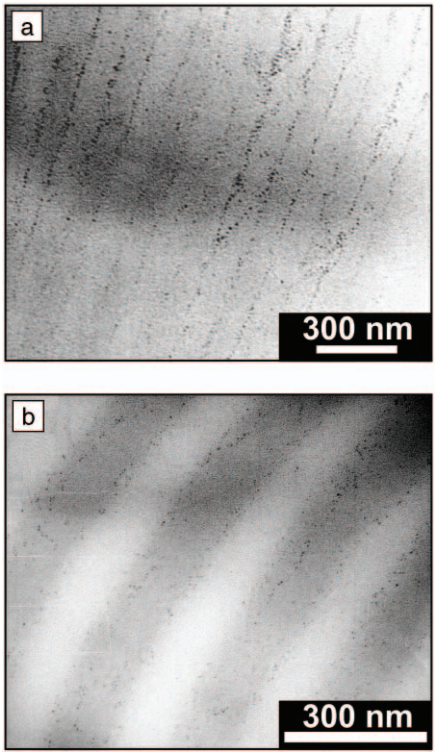

Figure 4. Bright-field transmission electron micrographs of an unstained block copolymer poly(styrene-b-ethylene/propylene)/nanocrystal (AuSPS or $AuSC_{18}H_{37}$) composite material after microsectioning normal to the layer direction, demonstrating (a) particle deposition at the intermaterial dividing surfaces ($PS–PEP/AuSC_{18}H_{37}$) and (b) homogeneous selective-layer morphology (PS–PEP/AuSPS), respectively. PEP domains appear as brighter regions in the micrograph. The volume filling fraction of gold for both samples is $\phi \approx 0.06$.

The thermodynamic prediction of BCP–nanoparticle phase diagrams is thus of importance in designing nanocomposites for applications. Balazs' group has combined density functional theory and self-consistent field theory to simulate the behavior of nanoparticles of diameter d in BCP domains of period L. They showed that the interfacial segregation of nanopar-

ticles with neutral ligands (i.e., $\chi = 0$) occurs for small particles ($d/L < 0.2$), whereas for $d/L \sim 0.3$, the particles locate in the center of the domain,[31–34] which was in reasonable agreement with experiments as well.[35,36] There are a host of parameters to explore concerning the localization of particles within BCP microdomains. These include the particle size and shape, ligand size and chemistry, and the size and shape of the particular host microdomain.[37] Information about the solubility limits of various particles in BCPs is the key in understanding the attainable limits to the effective dielectric constant via blending. Clearly, there is much still to be done to control the hierarchical structures in BCP–nanoparticle assemblies that can enhance nanocomposite photonic properties.

Switchable BCP Photonics

BCP-based photonic-bandgap materials that can be readily tuned or switched by applying various external fields can provide a route to the fabrication of multifunctional and optically responsive photonic structures. There is a host of ways to induce changes of optical properties via alteration of the periodicity, symmetry, or dielectric constants of the material.

Thermally tunable BCP-based photonic-bandgap materials have been constructed by incorporating *guest* liquid-crystalline molecules into one domain of *host* block copolymers by hydrogen-bonding interaction to form a hierarchical photonic structure.[38,39] Either the effective refractive index[38] or the lattice spacing[39] of liquid-crystal-containing domains could be changed as the temperature of the materials was changed, leading to the switching of the photonic stop band of the system.

Another way to alter the microdomain spacing in a BCP is to apply mechanical force. Elastomeric BCP photonic crystals have been prepared by blending with a nonvolatile plasticizer to form a BCP gel. The local deformation of the photonic gel's microstructure yields a tunable photonic bandgap with applied strains.[40] Figure 5 shows that the peak reflectivity of a lamellar block copolymer photonic gel can be altered by more than 100 nm with an applied strain of 100%.

Challenges, Advantages, and Applications

The concept of self-assembled BCP-based photonic materials has been successfully demonstrated. Advantages for employing self-assembled block copolymers for photonic applications include the ease of processing (e.g., conformal coatings on essentially any substrate); the ability to include both inorganic (e.g., quantum dots) and organic (e.g., laser dyes, homopolymers, plasticizers, etc.) materials within the BCP photonic crystal; and the fact that it is relatively easy to manipulate BCP photonic crystals via mechanical force, temperature, and electric fields.

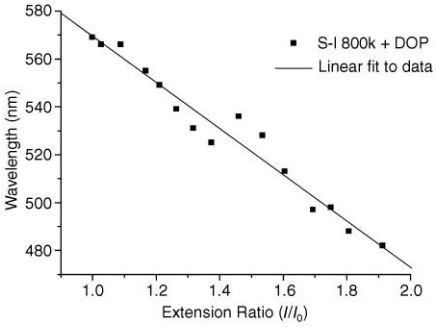

Figure 5. Peak reflectivity wavelength of a lamellar block copolymer photonic gel (800 kg/mol PS–PI block copolymer, S-I 800k, plasticized with dioctyl phthalate, DOP), plotted as a function of the measured deformation of the rubber substrate (represented as the extension ratio). The wavelength of peak reflectivity reversibly shifts to shorter values as the sample is stretched.

In order to maximize the usefulness of self-assembled BCP platforms, one has to address three major challenges: attaining large domain spacings, achieving high dielectric contrast, and controlling long-range microdomain order. The occurrence of randomly located defects that accompany the self-assembly process must be avoided. In this regard, there have been numerous efforts to establish a single-crystal-like microdomain structure, employing various external fields such as mechanical flow fields, electric fields, temperature gradients, directional solidification, and surface interactions to obtain purposefully long-range domain order during the self-assembly process.[1] However, the high-molecular-weight BCPs that are typical of photonic crystals present the problem that the order–disorder transition is unattainable via temperature, so solvents must be used to process the materials into their final structures, restricting the applicability of some of these techniques.

Somewhat surprisingly, we have found that the directional solidification process works very well for high-molecular-weight BCPs. Directional solidification uses a solvent that is actually a crystalline solid at room temperature and is only a good solvent above its melting temperature. For example, benzoic acid is a good solvent for both polystyrene and polyisoprene and melts at 123°C. When the benzoic acid is rapidly crystallized in a temperature gradient, the BCP domains align along the fast growth direction, resulting in large-area microdomain orientation in thin films.[41]

As mentioned in the introduction, the attainment of well-ordered photonic crystals is only one requirement. Actual useful optical devices need *controlled defects* to localize and guide light. One interesting application is the use of the self-assembled BCP photonic crystal to define a microcavity for modifying the spontaneous emission of optically active materials, ultimately leading to an optically pumped, all-organic, self-assembled laser. Clearly, 1D self-assembled photonic crystals from lamellar-forming BCPs can act as a Bragg reflector. Two different types of laser structures can then be envisioned: (1) a distributed-feedback band-edge laser and (2) a defect-mode microcavity laser. For the distributed-feedback structure, a gain medium such as an organic laser dye is dispersed throughout the layered BCP structure. In the defect-mode approach, a layer of precise dimension containing the gain medium is employed as the microcavity, sandwiched by outside BCP Bragg reflectors. In both cases, controlling the microdomain orientation of the BCP lamellae is the key to obtaining the high quality factor (a ratio of the energy stored in resonant cavity to the energy lost per cycle) that is essential to enable lasing.

Summary

This article reviewed the current status of photonic-bandgap materials based on block copolymers. We discussed the morphologies and optical properties of BCP-based photonic crystals and BCP–nanoparticle composites. One-, two-, and three-dimensional photonic crystals have been successfully demonstrated from lamellar-, cylinder-, and double-gyroid-forming diblock copolymers. Nanocomposite photonic materials based on BCPs and inorganic nanocrystals provide an essential way to enhance the inherent low dielectric contrast of neat BCPs. Examples of switchable BCP-based photonic materials using external stimuli such as thermal and mechanical forces have also been shown. Such systems have a potential for various sensor applications. The challenges in making BCPs more useful as photonic materials have been discussed, and these include attaining large domain periodicities, attaining a high dielectric contrast, controlling the long-range domain order, and purposefully introducing specific defects. Finally, promising applications such as self-assembled BCPs for all-organic, conformable lasers have been presented.

Acknowledgments

The MIT work in block copolymer photonics owes much to a host of talented graduate students and collaborators; in particular, Yoel Fink and Augustine Urbas were essential to launching our early efforts in photonic crystals. We also thank Chinedum Osuji, Chaitanya Ullal, Ion Bita, Peter DeRege, Martin Maldovan, Michael Bockstaller, and Tao Deng, as well as professors John Joannopoulos, Tim Swager, Chris Ober, Lewis Fetters, Paras Prasad, Craig Carter, and Moungi Bawendi. The authors would like to thank their respective financial sources: J. Yoon, the National Science Foundation for financial support under grant 0103297 (NSF–NIRT); W. Lee, the U.S. Air Force Defense University Research Initiative on Nanotechnology (DURINT) in conjunction with the University of Buffalo; E.L. Thomas, the NSF and DURINT as well as the Institute for Soldier Nanotechnologies under contract DAAD 19–02D0002 from the U.S. Army Research Office.

References

1. C. Park, J. Yoon, and E.L. Thomas, *Polymer* **44** (2003) p. 6725.
2. E.L. Thomas and R.L. Lescanec, *Philos. Trans. R. Soc. London, Ser. A* **348** (1994) p. 149.
3. A.C. Edrington, A.M. Urbas, P. DeRege, C.X. Chen, T.M. Swager, N. Hadjichristidis, M. Xenidou, L.J. Fetters, J.D. Joannopoulos, Y. Fink, and E.L. Thomas, *Adv. Mater.* **13** (2001) p. 421.
4. B. Temelkuran, S.D. Hart, G. Benoit, J.D. Joannopoulos, and Y. Fink, *Nature* **420** (2002) p. 650.
5. E. Chow, A. Grot, L.W. Mirkarimi, M. Sigalas, and G. Girolami, *Optics Lett.* **29** (2004) p. 1093.
6. M. Scalora, J.P. Dowling, C.M. Bowden, and M.J. Bloemer, *Phys. Rev. Lett.* **73** (1994) p. 1368.
7. J.D. Joannopoulos, R.D. Meade, and J.N. Winn, *Photonic Crystals: Molding the Flow of Light* (Princeton University Press, Princeton, 1995).
8. S. Noda, K. Tomoda, N. Yamamoto, and A. Chutinan, *Science* **289** (2000) p. 604.
9. M.H. Qi, E. Lidorikis, P.T. Rakich, S.G. Johnson, J.D. Joannopoulos, E.P. Ippen, and H.I. Smith, *Nature* **429** (2004) p. 538.
10. M. Campbell, D.N. Sharp, M.T. Harrison, R.G. Denning, and A.J. Turberfield, *Nature* **404** (2000) p. 53.
11. C.K. Ullal, M. Maldovan, M. Wohlgemuth, and E.L. Thomas, *J. Opt. Soc. Am. A: Opt. Image Sci. Vis.* **20** (2003) p. 948.
12. B.T. Holland, C.F. Blanford, and A. Stein, *Science* **281** (1998) p. 538.
13. P.V. Braun and P. Wiltzius, *Nature* **402** (1999) p. 603.
14. J. Wijnhoven and W.L. Vos, *Science* **281** (1998) p. 802.
15. Y. Fink, A.M. Urbas, M.G. Bawendi, J.D. Joannopoulos, and E.L. Thomas, *J. Lightwave Technol.* **17** (1999) p. 1963.
16. A. Urbas, Y. Fink, and E.L. Thomas, *Macromolecules* **32** (1999) p. 4748.
17. A. Urbas, R. Sharp, Y. Fink, E.L. Thomas, M. Xenidou, and L.J. Fetters, *Adv. Mater.* **12** (2000) p. 812.
18. P. Yeh, H. Yariv, and C. Shan, *J. Opt. Soc. Am.* **67** (1977) p. 423.
19. M. Born and E. Wolf, *Principles of Optics,* 7th ed. (Cambridge University Press, Cambridge, UK, 1999).
20. T. Deng, C.T. Chen, C. Honeker, and E.L. Thomas, *Polymer* **44** (2003) p. 6549.
21. E. Yablonovitch, *Phys. Rev. Lett.* **58** (1987) p. 2059.
22. S. John, *Phys. Rev. Lett.* **58** (1987) p. 2486.
23. E. Yablonovitch and T.J. Gmitter, *Phys. Rev. Lett.* **63** (1989) p. 1950.
24. H.S. Sozuer, J.W. Haus, and R. Inguva, *Phys. Rev. B* **45** (1992) p. 13962.
25. C.T. Chan, K.M. Ho, and C.M. Soukoulis, *Europhys. Lett.* **16** (1991) p. 563.
26. A.M. Urbas, M. Maldovan, P. DeRege, and E.L. Thomas, *Adv. Mater.* **14** (2002) p. 1850.
27. M. Maldovan, A.M. Urbas, N. Yufa, W.C. Carter, and E.L. Thomas, *Phys. Rev. B* **65** 165123 (2002).
28. M. Bockstaller, R. Kolb, and E.L. Thomas, *Adv. Mater.* **13** (2001) p. 1783.
29. M.R. Bockstaller and E.L. Thomas, *J. Phys. Chem. B* **107** (2003) p. 10017.
30. M.R. Bockstaller and E.L. Thomas, *Phys. Rev. Lett.* **93** 166106 (2004).
31. J. Huh, V.V. Ginzburg, and A.C. Balazs, *Macromolecules* **33** (2000) p. 8085.
32. R.B. Thompson, V.V. Ginzburg, M.W. Matsen, and A.C. Balazs, *Science* **292** (2001) p. 2469.
33. J.Y. Lee, R.B. Thompson, D. Jasnow, and A.C. Balazs, *Macromolecules* **35** (2002) p. 4855.
34. G.A. Buxton, J.Y. Lee, and A.C. Balazs, *Macromolecules* **36** (2003) p. 9631.
35. M.R. Bockstaller, Y. Lapetnikov, S. Margel, and E.L. Thomas, *J. Am. Chem. Soc.* **127** (2003) p. 5276.
36. J.J. Chiu, B.J. Kim, E.J. Kramer, and D.J. Pine, *J. Am. Chem. Soc.* **127** (2005) p. 5036.
37. M.R. Bockstaller, R.A. Mickiewicz, and E.L. Thomas, *Adv. Mater.* **17** (2005) p. 1331.
38. C. Osuji, C.Y. Chao, I. Bita, C.K. Ober, and E.L. Thomas, *Adv. Funct. Mater.* **12** (2002) p. 753.
39. S. Valkama, H. Kosonen, J. Ruokolainen, T. Haatainen, M. Torkkeli, R. Serimaa, G. Ten Brinke, and O. Ikkala, *Nature Mater.* **3** (2004) p. 872.
40. A. Urbas, "Block Copolymer Photonic Crystals," PhD Thesis, Massachusetts Institute of Technology (2003).
41. C. De Rosa, C. Park, B. Lotz, J.C. Wittmann, L.J. Fetters, and E.L. Thomas, *Macromolecules* **33** (2000) p. 4871. □